Pressure-induced structural and magnetic phase transitions in La$_{0.75}$Ba$_{0.25}$CoO$_{2.9}$ studied with scattering methods and first-principle calculations

M. Feygenson [1,2] D. Y. Novoselov [3,4] M. A. Mazannikova [3,4] D. M. Korotin [3] M. Bushinsky [5] D. Karpinsky [5]
M. Hanfland [6] A. Sazonov [7] S. Savvin [8] F. Porcher [9] R. Svetogorov [10] A. Veligzhanin [10] S. Tiutiunnikov [10]
S. Arumugam [11] and V. Sikolenko [12,13,14,*]

[1]*European Spallation Source ERIC, P.O. Box 176, SE-221 00, Lund, Sweden*
[2]*Forschungszentrum Jülich GmbH, Jülich Centre for Neutron Science (JCNS-1), D-52425 Jülich, Germany*
[3]*M.N. Mikheev Institute of Metal Physics UB RAS, 620137, S. Kovalevskaya str. 18, Ekaterinburg, Russia*
[4]*Department of theoretical physics and applied mathematics, Ural Federal University, Mira St. 19, 620002 Yekaterinburg, Russia*
[5]*Scientific-Practical Materials Research Centre of NAS of Belarus, 220072 Minsk, Belarus*
[6]*European Synchrotron Radiation Facility, BP 220, 38043 Grenoble, France*
[7]*European Spallation Source (ESS) ERIC, Data Management and Software Centre (DMSC), 2200 Copenhagen, Denmark*
[8]*Institut Laue-Langevin, 71 avenue des Martyrs, CS 20156, 38042 Grenoble cedex 9, France*
[9]*CEA Saclay Laboratoire Léon Brillouin F-91191 Gif Sur Yvette, France*
[10]*NRC "Kurchatov Institute", Acad. Kurchatov sq. 1, 123182 Moscow, Russia*
[11]*Centre for High Pressure Research School of Physics Bharathidasan University Tiruchirappalli 620 024, India*
[12]*Joint Institute for Nuclear Research, 141980 Dubna, Russia*
[13]*Karlsruhe Institute of Technology, 76131 Karlsruhe, Germany*
[14]*REC Functional Nanomaterials, Immanuel Kant Baltic Federal University, Kaliningrad 236041, Russia*

We studied structural and magnetic phase transitions under applied pressure for the doped cobaltite La$_{0.75}$Ba$_{0.25}$CoO$_{2.9}$. Neutron and x-ray diffraction experiments established the coexistence of rhombohedral and cubic phases in the sample. The magnetic state at 2 K is best described as a long-range ordered antiferromagnet (AFM) with small ferromagnetic (FM) clusters. With application of pressure, the rhombohedral phase gradually transforms into a cubic one. At room temperature and the highest applied pressure of 16 GPa, the cubic phase accounts for 70% of the sample volume. Quantum mechanical modeling confirmed the experimental findings and provided more insights into the structural and magnetic phase transitions at pressures exceeding 16 GPa. While the cubic crystal structure was preserved above 10 GPa, the AFM to FM phase transition was found at around 16 GPa. Further increase of the pressure resulted in suppression of magnetic order above 45 GPa. Using density functional theory (DFT)+U calculations, we were able to relate macroscopic magnetic properties induced by pressure with corresponding spin-state transitions in Co ions.

I. INTRODUCTION

The spin-state transitions of Co ions in cobalt oxides with pervoksite structure (cobaltites) have been intensively studied by experimental and computational methods [1–8]. The most studied cobaltite LaCoO$_3$ displays thermally induced transitions of Co^{3+} from low spin (LS) state to intermediate spin (IS) and high spin (HS) states due to the competition between crystal-field splitting Δ_{cf} and Hund's rule exchange balance [9]. The crystal-field splitting is rapidly increasing with decreasing Co-O bond length r ($\Delta_{cf} \sim r^{-5}$); thus, variations of Co-O bond length can induce a spin-state transition. The most straightforward way of increasing Co-O bond is to increase the temperature; yet even in this case, the exact mechanisms of the thermally induced spin-state transitions in LaCoO$_3$ are still under debate. At the same time, other ap-

proaches to change Co-O bond length and the corresponding spin-state transitions were employed, such as doping, external pressure, and application of high magnetic fields [10–17]. While adding external parameters complicates understanding of the spin-state transitions in cobaltites, it offers many fascinating opportunities to engineer new types of materials with unique transport and magnetic properties. In this work, we focus on a partial substitution of La^{3+} with the alkaline-earth metal Ba^{2+}. Ba^{2+} has a larger ionic radius of 149 pm, as compared with the radius of 106 pm for La^{3+} ion. The parent LaCoO$_3$ compound crystallizes into a perovskite structure with rhombohedral distortions with the space group $R\bar{3}c$ in a wide range of temperatures and pressures [1]. Replacing La atoms with Ba reduces these distortions, and further application of external pressure could potentially stabilize such undistorted cubic phase (space group $Pm\bar{3}m$). There is a large number of articles devoted to theoretical modeling of the electronic structure of LaCoO$_3$ [9,18–29]; yet there are much fewer works on calculations of its doped

compositions [30–32], partially due to difficulties in the direct numerical modeling of nonstoichiometric compositions that require supercells with a large number of atoms. Furthermore, analysis and interpretation of all possible configurations of impurity atom positions is very complex. The studies of the doped compositions areimportant not only for revealing their novel properties but also for a deeper understanding of structural, magnetic, and spin-state transitions in $LaCoO_3$, not to mention the intriguing IS state of cobalt ions in these compounds.

Ba doping leads to a formation of cobalt ions having an oxidation state of 4+ that consequentially modifies magnetic properties of the doped cobaltite. The exchange interactions between Co^{3+} and Co^{4+} ions are positive and responsible for the formation of a long-range ferromagnetic (FM) order in alkali-doped cobaltites [10–12]. Magnetic properties of the compounds lightly doped with alkali-earth elements are mainly characterized by a coexistence of both FM and antiferromagnetic (AFM) phases caused by competitive positive and negative exchange interactions formed between the cobalt ions. In particular, $La_{0.5}Ba_{0.5}CoO_{2.87}$ and $La_{0.75}Ba_{0.25}CoO_3$ compounds have the same nominal ratio of Co^{3+}/Co^{4+}, but different magnetic properties. It is a clear indication that ionic size effect and structural distortions are additional factors, which determine magnetic properties of these compounds. Thus, samples with different structural parameters retaining their cobalt ions in dominant 3+ oxidation state are excellent model systems. They can be used to clarify an origin of various magnetic properties depending on Co-O chemical bond geometry, as well as the effect of external parameters such as pressure and temperature.

Application of an external pressure is an elegant tool for manipulating the electronic structure of materials without affecting their composition. Previous studies of 2D and 3D pervoskites showed that phase transformations, band-gap shifts, variations in electronic conductivity, piezochromism, and half-metallicity could be induced by applying pressure [33–40]. Particularly for cobaltites, an external pressure modifies the crystal structure by changing Co-O bond length and/or Co-O-Co bond angle, resulting in emerging novel electronic and magnetic properties. However, there are only a few experimental reports on the high-pressure diffraction studies of Ba-doped cobaltites. For oxygen-deficient $La_{0.5}Ba_{0.5}CoO_{2.87}$ compound, application of a moderate pressure up to 4.3 GPa at low temperatures resulted in suppression of the AFM order and an increase of spontaneous magnetization and T_C for the FM phase [41–43]. For the sample with a lower Ba-doping and nominal O content ($La_{0.75}Ba_{0.25}CoO_3$), application of pressure resulted in the suppression of FM phase with a significant reduction of the magnetic moment at 50 K and 8 GPa down to $0.7\mu_B$ per Co from a value of $1.65\mu_B$ at the same temperature under ambient pressure. Such dramatic reduction in the magnitude of magnetic moment was explained by the pressure-induced spin-state transition from IS to LS of the Co ions [44]. Experiments have established that Ba-doped cobaltites exhibit a plethora of nontrivial transport and magnetic properties under high pressure, which has become the focus of our study.

We present here the results of experimental and theoretical studies of the structural and magnetic phase transitions

in the $La_{0.75}Ba_{0.25}CoO_{2.9}$ compound having dominant cobalt ions in 3+ oxidation state as a function of applied pressure and temperature. The magnetic structure was obtained from neutron-scattering experiments at various temperatures and ambient pressure. The crystal structure as a function of applied pressure of up to 16 GPa was studied using synchrotron x-ray diffraction. In order to interpret our experimental data and elucidate the physics underlying observed phase transitions, we performed DFT+U calculations of the parent compound taking into account the steric effect caused by the substantial difference of the ionic radii of La and Ba to model the phase transitions in the nonstoichiometric composition. Our results revealed a relation between spin-state transitions induced by applied pressure and macroscopic magnetic properties of the $La_{0.75}Ba_{0.25}CoO_{2.9}$ compound.

II. EXPERIMENTAL AND CALCULATIONAL DETAILS

The ceramic sample of $La_{0.75}Ba_{0.25}CoO_{2.9}$ was synthesized by conventional solid-state reaction technique as described in Ref. [45]. The high-purity oxides La_2O_3, Co_3O_4 and carbonate $BaCO_3$ were taken in stoichiometric ratio and thoroughly mixed in a planetary mill Retsch PM100 at 300 rpm for 30 min. The preliminary annealing was performed at 1000°C for 2 h and the obtained product was thoroughly grounded. The final synthesis was performed at 1200°C for 8 h. The sample was cooled from 1200°C to 300°C at a rate of 100°C per hour. The nominal chemical composition of the sample was confirmed by Rietveld refinements of neutron and synchrotron x-ray diffraction data at ambient conditions. Neutron-diffraction measurements revealed the oxygen content of 2.90(2).

The high-pressure x-ray diffraction measurements were performed at the beamline ID09A of the European Synchrotron Radiation Facility. Using the membrane-type diamond anvil cells, the highest pressure of 16 GPa was achieved. The low-temperature measurements were carried out in an He-flow cryostat at 50, 150, and 300 K using a wavelength of 0.41 Å. The measurements were done by varying pressure at constant temperature. A MAR555 flat panel detector was used to collect the data.

The neutron-diffraction experiments for the $La_{0.75}Ba_{0.25}CoO_{2.9}$ sample were performed using the high-resolution powder diffractometer D2B at the Institute Laue-Langevin with neutron wavelengths of 1.59 and 1.05 Å, in the dedicated cryostat from 2 to 300 K over the angular range from 5 to 150 degrees. The reference $LaCoO_3$ sample was measured at 3T2 beamline at Laboratoire Léon Brillouin, France. The data were collected at $\lambda = 1.23$ Å in the angular range from 4.5 to 121 degrees at various temperatures from 2 to 1000 K. The experimental data were analyzed by the Rietveld method using the FullProf software package.

The standard field-cooled (FC) and zero-field-cooled (ZFC) measurements of the temperature-dependent DC magnetization were carried out in a field of 200 Oe using the Physical Property Measurement System (PPMS).

The first-principles calculations were performed in the framework of the DFT using the Vienna *ab-initio* simulation package (VASP) [46]. Strong electronic correlations on the 3d-states of Co ions were taken into account using
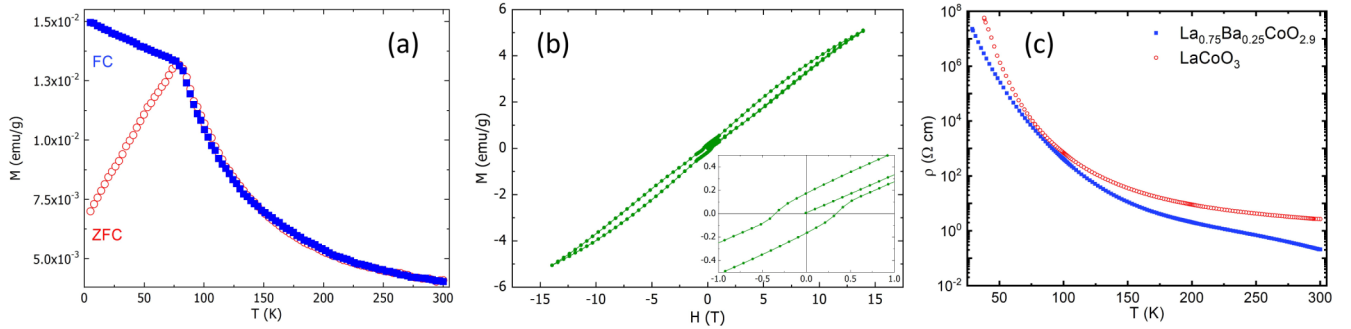
FIG. 1. (a) Temperature-dependent ZFC and FC magnetizations for $La_{0.75}Ba_{0.25}CoO_{2.9}$, measured in an applied magnetic field of 200 Oe. (b) Field-dependent ZFC magnetization measured at 5 K. Inset: The same plot at lower fields showing the finite coercive field of about 0.4 T. (c) Temperature-dependent resistivity measurements in zero field for $La_{0.75}Ba_{0.25}CoO_{2.9}$ and $LaCoO_3$ samples.

the DFT+U method with Hubbard correction parameter U = 6 eV and exchange parameter J = 0.8 eV [8]. Two space groups $Pm\bar{3}m$ and $R\bar{3}c$ were considered. Calculations for the $Pm\bar{3}m$ phase were carried out for the unit cell doubled in each direction. The full symmetry of the system, with the exception of the magnetic subsystem, was preserved. The least-squares approximation was used in order to construct the total energies volume dependencies. Calculations were made in the non-spin-polarized mode, as well as with the spin polarization with FM and AFM long-range order.

III. RESULTS

A. Magnetization and resistivity measurements

The results of the magnetization measurements with the PPMS system are displayed in Fig. 1. The bifurcation of the FC and ZFC magnetizations below ∼85 K directly confirms the presence of a FM phase in our sample [Fig. 1(a)]. Such temperature dependence is typical for small FM clusters being blocked at temperatures below so-called blocking temperature. The same phenomena of magnetic blocking was observed for FM nanoparticles embedded into an AFM matrix [47,48]. Below the blocking temperature there is insufficient thermal energy in equilibrium to completely reverse the magnetic moment of a nanoparticle or cluster. As the temperature increases, thermal fluctuations induce the gradual alignment of FM clusters along the applied magnetic field, and the ZFC magnetization increases monotonously up to the blocking temperature.

Figure 1(b) shows the full-magnetization loop $M(H)$ after cooling from room temperature to 5 K in zero field. The magnetization of the $La_{0.75}Ba_{0.25}CoO_{2.9}$ sample shows no saturation even at the field as high as 14 T. The hysteresis loop with a coercivity field of ∼0.4 T is visible at 5 K, below the blocking temperature. Nonsaturating magnetization and linearlike loop are characteristic for the presence of a dominating AFM phase in our sample. The finite coercive field, however, suggests the presence of FM clusters, consistent with our FC and ZFC magnetization measurements.

We further investigated the evidence of the AFM phase with FM clusters by carrying out resistivity measurements. Figure 1(c) compares the resistivity ρ for the $La_{0.75}Ba_{0.25}CoO_{2.9}$ and reference $LaCoO_3$ samples. The temperature dependence of ρ is qualitatively similar for both

samples, indicative of an insulator with ρ rapidly increasing on cooling. The resistivity of $La_{0.75}Ba_{0.25}CoO_{2.9}$ sample is significantly lower, reaching the magnitude of at least 20 times smaller compared with $LaCoO_3$ sample at low temperatures. Previous studies concluded that the insulating behavior of ρ was related to the AFM phase, while the FM phase was attributed to a conducting behavior [16,41,49]. In agreement with magnetization measurements, the reduction of ρ in $La_{0.75}Ba_{0.25}CoO_{2.9}$ is associated with a presence of a minor FM phase in the dominant AFM phase.

B. Neutron powder diffraction

Neutron powder diffraction was used to provide independent measurements of the crystal and magnetic structures of our sample on atomic scale. Both $La_{0.75}Ba_{0.25}CoO_{2.9}$ and the parent $LaCoO_3$ compounds were measured under ambient pressure. Figure 2(a) shows the Rietveld refinement of the neutron-diffraction data collected at 2 K for $La_{0.75}Ba_{0.25}CoO_{2.9}$. In order to refine 2 K data, we used a model for the crystal and magnetic structures previously reported for the samples of similar composition [17,44]. This model can account for the coexistence of FM and AFM phases that were indicated by our magnetization and resistivity measurements. The best fit with $\chi^2 = 0.838$ was obtained using two crystal (rhombohedral and cubic) and two magnetic (AFM and FM) phases. The coexistence of FM and AFM phases agrees with our magnetization and resistivity measurements. The rhombohedral phase was described using the space group $R\bar{3}c$ with $\sqrt{2}a_p \times \sqrt{2}a_p \times 2\sqrt{3}a_p$ superstructure (a_p is a primitive perovskite lattice parameter), while the cubic phase was described using the space group $Pm\bar{3}m$. We note that sensitivity of our neutron data to the cubic phase at 2 K is rather limited, because similar $\chi^2 = 0.839$ was achieved when this phase was excluded from the Rietveld refinement. However, the presence of the cubic phase was unambiguously confirmed by high-resolution synchrotron x-ray measurements (see next section) and by neutron diffraction at room temperature; thus, for the sake of consistency, the fit with four phases is shown in Fig. 2(a).

The AFM phase is described by using the space group $P1$ with g-type AFM ordering [50] with propagation vector $k = (\frac{1}{2}\frac{1}{2}\frac{1}{2})$ and six Co atoms positioned according to the space group. The Rietveld refinements at room temperature
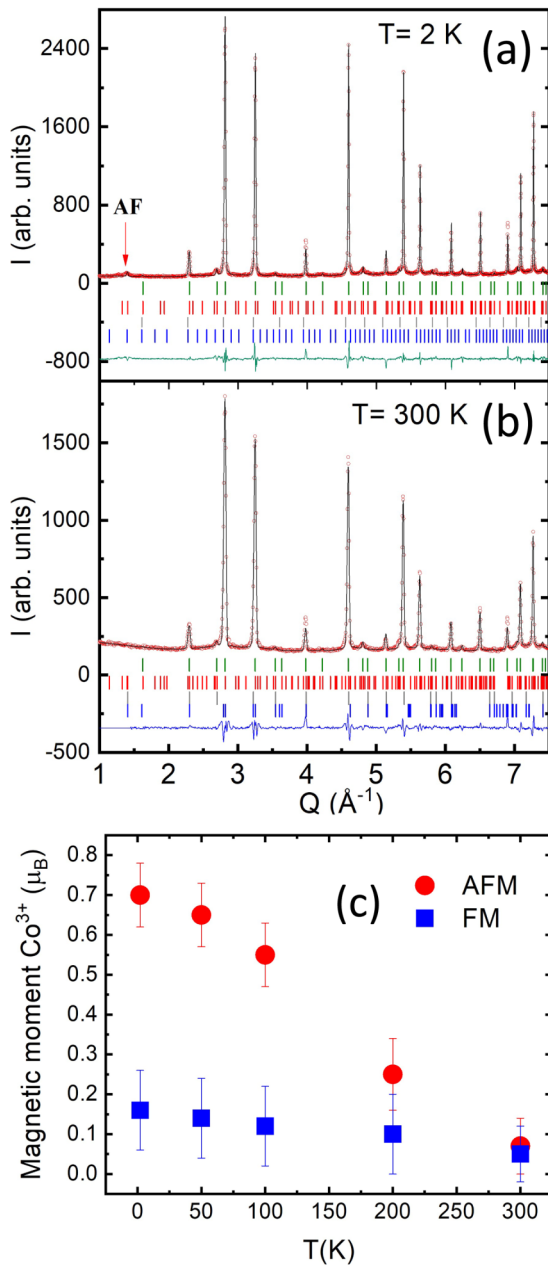
FIG. 2. The Rietveld refinement of the neutron-diffraction data for $La_{0.75}Ba_{0.25}CoO_{2.9}$ measured at 2 K (a) with $\lambda = 1.59$ Å and at 300 K (b) with $\lambda = 1.05$ Å. The experimental data are in open circles, the calculated pattern is in blue, and the difference curve is in green. The tick marks indicate Bragg peak positions for $Pm\bar{3}m$ (gray), $R\bar{3}c$ (green), FM (blue), and AFM (red) phases. (c) The magnetic moment of Co^{3+} for separate AFM and FM phases as a function of temperature.

indicated a coexistence of rhombohedral (85%) and cubic (15%) phases [Fig. 2(b)]. The quality of refinements was notably improved by adding a FM phase associated with Co atoms with magnetic moments ordered along the c direction of the rhombohedral lattice. Based on the obtained results, the FM moment remains nearly stable in the temperature range 5–300 K [Fig. 2(c)]. This result agrees with DC magnetization measurements that indicated a small amount of

FM phase [Figs. 1(a) and 1(b)] at low temperatures. Above the blocking temperature the presence of FM clusters is not evident from DC magnetization data, and additional x-ray magnetic circular dichroism measurements are needed to confirm neutron-diffraction results. Using chemical composition of our sample and principle of electroneutrality, we deduced that the sample consists of 95% Co^{3+} and 5% Co^{4+}. The hysteresis loop with a small coercivity field is likely a result of positive exchange interactions between Co^{4+} and Co^{3+} ions. A small fraction of Co^{4+} ions is unavoidable formed because of uncertainty in oxygen content during the sample preparation process. The value of FM moments calculated based on isothermal magnetization dependencies and neutron-diffraction measurements is about 0.16(10) μ_B, which is close to the accuracy of the neutron-diffraction method.

We compare the temperature dependence of the Co-O bond length and its mean-square displacement (MSD) for $La_{0.75}Ba_{0.25}CoO_{2.9}$ and $LaCoO_3$ samples in Fig. 3. The results for $La_{0.75}Ba_{0.25}CoO_{2.9}$ indicate a regular thermal expansion with both Co-O bond length and MSD gradually increasing with the temperature. The situation is different for the parent compound $LaCoO_3$, in which both values show first decrease as a function of the increasing temperature up to 50 K. The origin of this effect is described in detail in our previous work [8].

C. Synchrotron x-ray diffraction under high pressure

The synchrotron x-ray diffraction measurements were used to study the structural transitions in $La_{0.75}Ba_{0.25}CoO_{2.9}$ induced by applying pressure up to 16 GPa at T= 50, 150, and 300 K. The overall quality of our data is presented in Fig. 4. This figure shows the Rietveld refinement of the data collected at the highest pressure of 16 GPa at 50 K. The signal-to-background ratio is high and the background is featureless.

We started with the Rietveld refinement of the data collected at ambient conditions using the crystal structure obtained from the room-temperature neutron-diffraction experiments. The Rietveld refinement confirmed the coexistence of two phases. In agreement with our neutron-diffraction experiments, we found that the major rhombohedral phase (80%) is described by the space group $R\bar{3}c$ and the second minor phase (20%) is cubic with the space group $Pm\bar{3}m$. When pressure is applied, the unit-cell volume of both phases is gradually decreasing [Figs. 5(a) and 5(b)]. A dip in the cell volume is observed at around 7–10 GPa for both phases at 50 K. The Co-O bond length shows qualitatively similar pressure dependence, with a dip in the same pressure range [Figs. 5(c) and 5(d)].

Figure 6 depicts the temperature and pressure dependence of the cubic phase fraction. The cubic phase fraction is gradually increasing at all temperatures. The cubic phase fraction at 300 K reaches a maximum value of 70% at the highest applied pressure of 16 GPa.

D. Electronic structure calculations

Our diffraction measurements confirmed that $R\bar{3}c$ is the main phase of $La_{0.75}Ba_{0.25}CoO_{2.9}$ at 2 K and ambient pressure. DFT+U calculations were carried out in order to
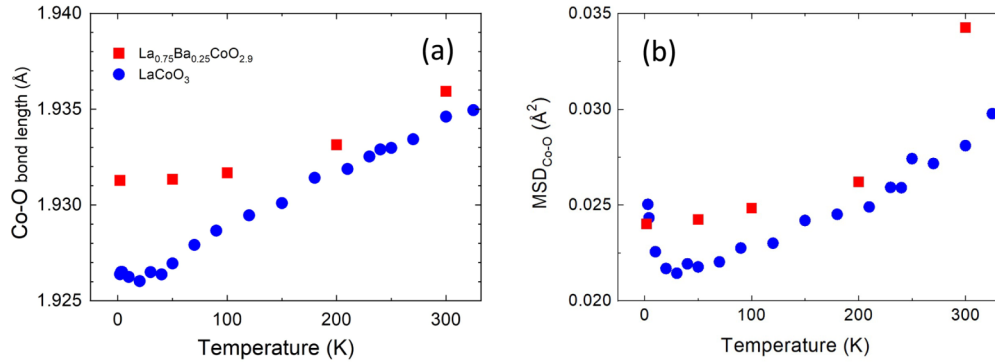
FIG. 3. The temperature dependence of (a) Co-O bond length and (b) MSD of Co-O bond, both obtained from the Rietveld refinement of the neutron powder diffraction data for $La_{0.75}Ba_{0.25}CoO_{2.9}$ and $LaCoO_3$ samples.

investigate pressure-induced structural and magnetic phase transitions at 0 K and compare them with the parent compound. The oxygen deficiency does not significantly affect the structural stability of the $La_{1-x}Ba_xCoO_{3-\delta}$ system with randomly distributed Ba cations at $x > 0.35$ [17,32,51–53]. Therefore, we consider the key factor responsible for the structural transition from rhombohedral to cubic phase under pressure to be a steric effect caused by a change in the effective ionic radius of the La and Ba cations.

The unit-cell volume per atom for $R\bar{3}c$ and $Pm\bar{3}m$ structures in the doped sample is increased by 0.1453 $Å^3$/atom at 0 GPa compared with the parent compound $LaCoO_3$. The difference is further increased to 0.268 $Å^3$/atom, when the external pressure of 16 GPa is applied. This effect was approximated by the shift of the energy per volume dependencies for these phases relative to each other by the corresponding difference in the volumes, and it was taken into account in our DFT+U calculations for the parent compound $LaCoO_3$. Figure 7(a) shows a structural transition from the $R\bar{3}c$ to the $Pm\bar{3}m$ phase near 10.6 $Å^3$/atom. When pressure increases
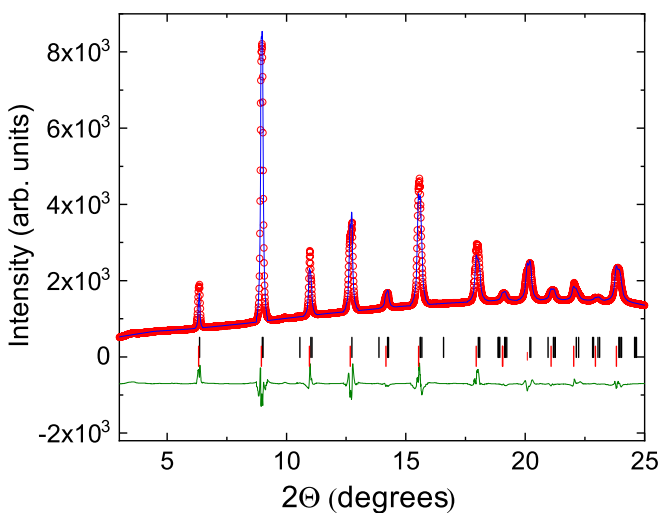

FIG. 4. The Rietveld refinement of the synchrotron x-ray diffraction data for $La_{0.75}Ba_{0.25}CoO_{2.9}$ measured at 50 K and 16 GPa, with experimental data in open circles, the calculated pattern in blue, and the difference curve in green. The tick marks indicate Bragg peak positions for $R\bar{3}c$ (black) and $Pm\bar{3}m$ (red) phases.

further, the magnetic phase transition from AFM to FM order within $Pm\bar{3}m$ symmetry occurs at about 10.3 $Å^3$/atom, corresponding to 16 GPa. The AFM-FM phase transition becomes evident once the differences in the total energies between $Pm\bar{3}m$ (AFM, FM) and $R\bar{3}c$ (AFM) are calculated as a function of the unit-cell volume [Fig. 7(b)]. This result further reinforces our conclusion that application of pressure to $La_{0.75}Ba_{0.25}CoO_{2.9}$ sample leads to the structural transition from the rhombohedral ($R\bar{3}c$) to the cubic ($Pm\bar{3}m$) phase with stabilization of FM order. Moreover, according to our calculations, further compression leads to the nonmagnetic (NM) state of the entire system with the unit-cell volume per atom below 9.26 $Å^3$/atom (above 45 GPa).

In order to understand the origin of phase transitions in our sample induced by pressure, we investigated the accompanying spin-state transitions. This was done by calculating density of states (DOS) of three distinctive magnetic configurations induced by pressure. We started with the DOS calculations for the NM phase that appeared when unit-cell volume is compressed below 9.26 $Å^3$/atom, roughly corresponding to applied pressure of 45 GPa [see Fig. 7(b)]. Figures 8(a) and 8(b) show total and partial DOS calculated at $V = 8.96$ $Å^3$/atom for NM. According to our calculations NM is in insulating ground state characterized by a 0.8 eV gap between fully occupied t_{2g} and half-filled e_g sublevels. The DOS of the AFM phase with $V = 11.51$ $Å^3$/atom revealed the gap of about 1.16 eV [Figs. 8(c) and 8(d)]. This solution corresponds to the HS state configuration of Co ions with the magnetic moments about 3.1 μ_B. The IS state at $V = 11.18$ $Å^3$/atom in the FM phase turns out to be metallic [Figs. 8(e) and 8(f)], i.e., weak band splitting prevents formation of the energy gap for the IS state with cobalt ions having magnetic moments of about 2.1 μ_B. These results are in qualitative agreement with the DOS characteristics of HS, LS, and IS spin-states in the parent compound $LaCoO_3$, previously reported by Korotin *et al.* [9].

IV. DISCUSSION

Before we begin our discussion of the physical origin of spin-state transitions under high pressure, we will summarize the structural and magnetic properties of $La_{0.75}Ba_{0.25}CoO_{2.9}$ at ambient pressure. The magnetization and resistivity measurements imply that below 85 K, the magnetic state of
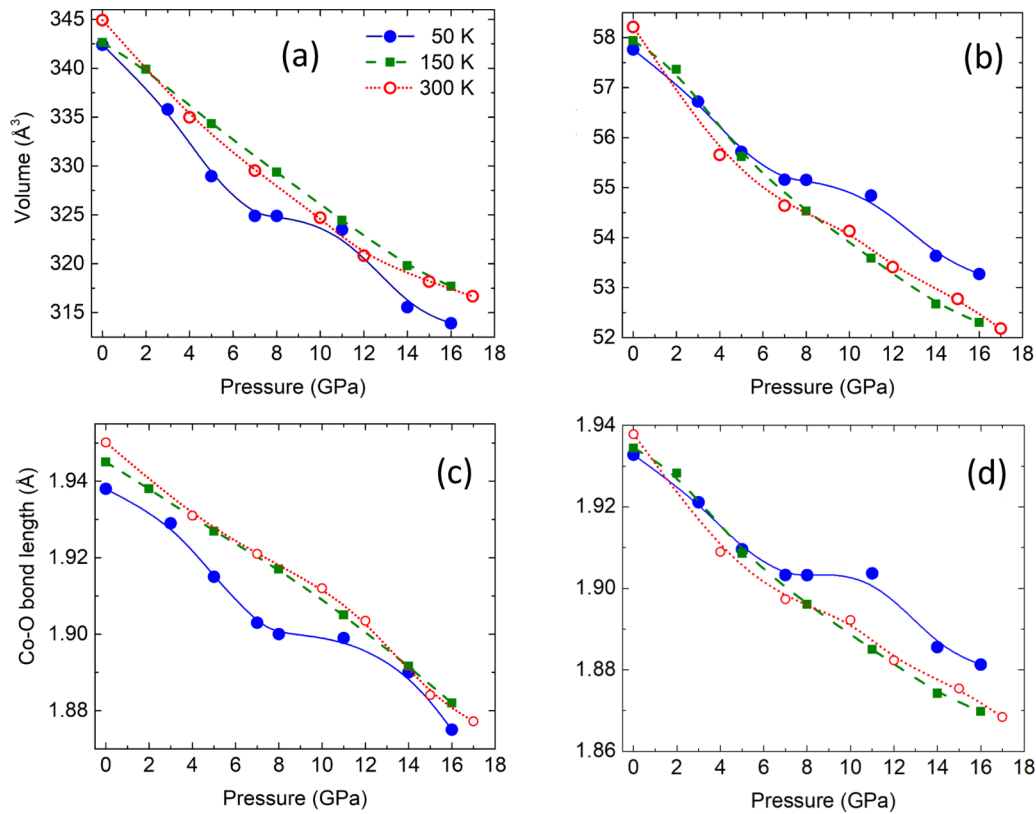
FIG. 5. The pressure dependence of the unit-cell volume for the rhombohedral (a) and cubic (b) phases at various temperatures. Corresponding Co-O bond length for the rhombohedral (c) and cubic (d) phases at the same temperatures. The lines are guides for the eye.

our sample is best described as a mixture of AFM and FM phases. The FM phase is presumably in the form of small clusters with a strong magnetic anisotropy characteristic for FM nanoparticles. This result was independently confirmed by the neutron-diffraction measurements that established the presence of both AFM and FM phases in our sample at low temperatures. Moreover, a much lower magnetic moment of Co^{3+} ions in the FM phase as compared with the AFM phase

FIG. 6. The volume of the cubic phase fraction as a function of applied pressure at various temperatures.

is a clear indication that the FM phase is minor. For the doped cobaltites, the presence of small FM clusters embedded into the AFM matrix was also experimentally confirmed by magnetization measurements, small-angle neutron scattering, electron microscopy, and nuclear magnetic resonance studies [54,55]. The FM clusters are presumably formed by the FM double-exchange between Co^{3+} and Co^{4+} ions. Interestingly, samples with full oxygen content $La_{0.8}Ba_{0.2}CoO_3$ and $La_{0.7}Ba_{0.3}CoO_3$ showed the long-range FM order with a large coercive field and saturating $M(H)$ [12]. We must conclude that the oxygen deficiency stabilizes AFM order in our sample, which is due to superexchange interactions between Co^{3+} and Co^{3+} and/or Co^{4+} and Co^{4+} [56].

At room temperature and ambient pressure, the crystal structure of our sample is a mixture of dominant rhombohedral ($R\bar{3}c$) and cubic ($Pm\bar{3}m$) crystal structures. When pressure is applied at low temperature, the rhombohedral structure is gradually transforming into the cubic one. At the lowest temperature of 50 K and the highest pressure of 16 GPa accessible in our x-ray diffraction experiment, the rhombohedral phase dominates until the cubic phase reaches about 50% of the sample volume.

We have extended the studies of applied pressure on the crystal structure transitions by carrying out electronic structure calculations. These calculations not only allowed us to predict the structural behavior of our sample at pressures exceeding the experimental ones but also allowed us to identify the magnetic order and the spin-state of Co ions in each phase. The studies of the total energy of various magnetic configurations as a function of the unit-cell volume revealed
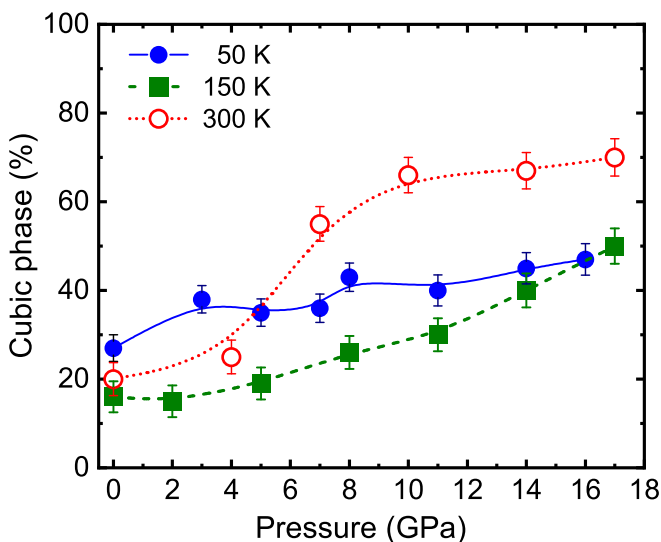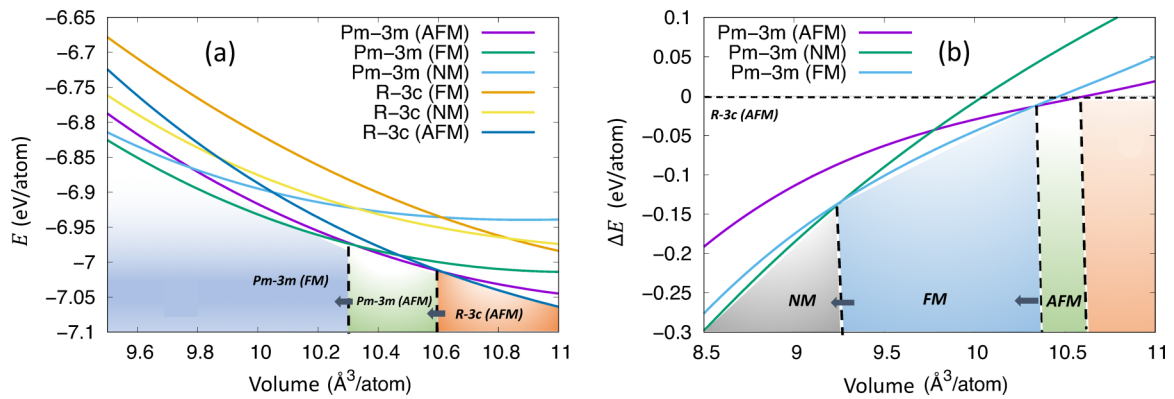
FIG. 7. (a) The energy of different magnetic configurations for as a function of the unit-cell volume. (b) The dependence of the difference ΔE of total energies on the volume between $Pm\bar{3}m$ (AFM, FM) and $R\bar{3}c$ (AFM) magnetic states. The vertical dashed lines correspond to the phase transitions.

that the structural transition from rhombohedral to cubic phase at applied pressure of about 10 GPa ($V = 10.6$ Å^3/atom) preserves AFM order of the sample. After the pressure of 16 GPa ($V = 10.3$ Å^3/atom) is applied, an AFM to FM order transition takes place within the same cubic crystal structure ($Pm\bar{3}m$). With further increase of pressure the sample remains cubic; however, at about 45 GPa ($V = 9.26$ Å^3/atom), the magnetic order is completely suppressed.
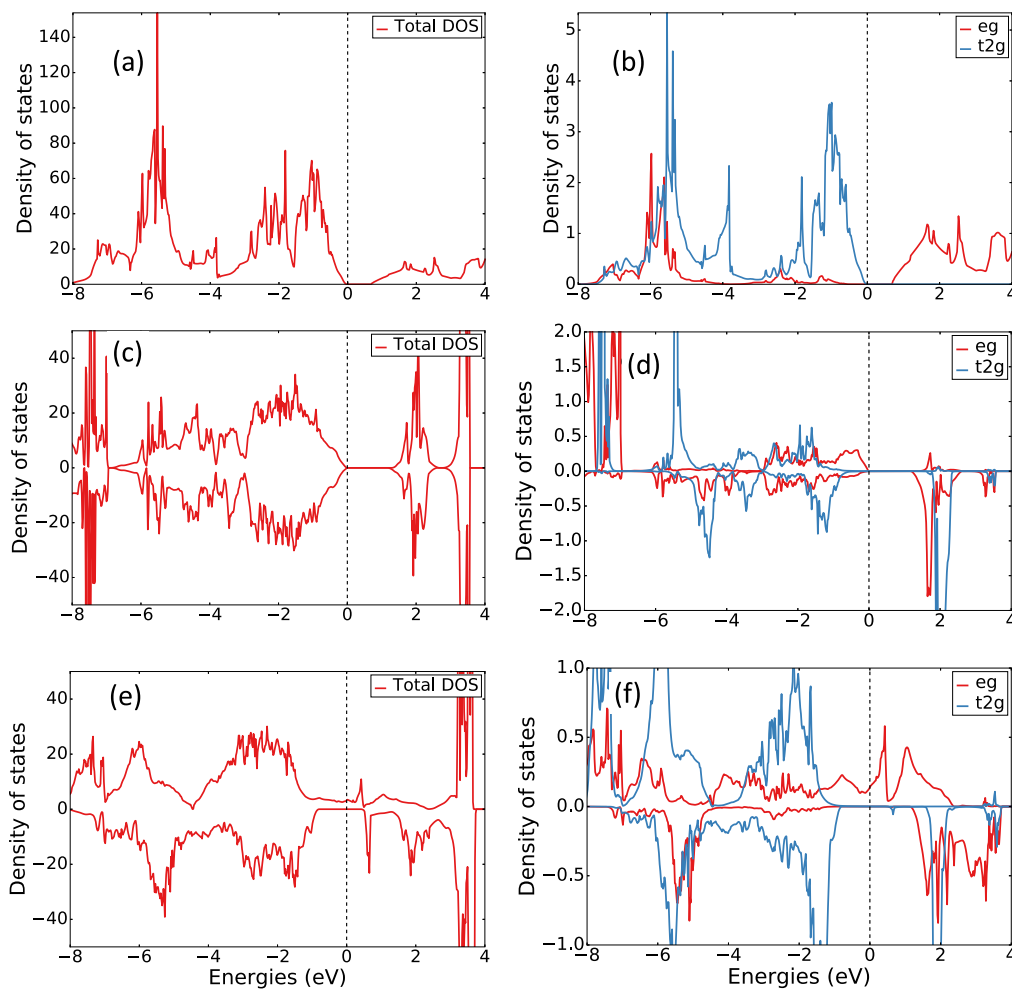

FIG. 8. Total and partial densities of states for (a), (b) $Pm\bar{3}m$ (NM) at V = 8.96 Å^3/atom (LS state), for (c), (d) $Pm\bar{3}m$ (AFM) with V = 11.51 Å^3/atom (HS state), and for (e), (f) $Pm\bar{3}m$ (FM) at $V = 10.18$ Å^3/atom (IS state). Zero energy corresponds to the Fermi energy. Positive and negative values of DOS correspond to spin-up and spin-down.

We continue our discussion by attributing the spin-states of Co ions in different magnetic phases and consequentially describing the spin-state transitions induced by applied pressure. Our DOS calculations of LS, IS, and HS states show that only the IS state is metallic due to the spin-orbital ordering. Despite very different ionic radius of LS and HS states, they are nonconducting and might be ascribed to AFM or NM ordering. The NM solution at high pressure is characterized by the presence of a small energy gap between the t_{2g} and the e_g sublevels arising from splitting by a strong crystal field. In addition, the presence of a gap may be associated with a slight overestimation of the localization degree of electrons in a partially filled cobalt d-shell, which is an artifact of the DFT+U method. The Co-O bond length and its MSD both show monotonous increase with temperature, which in contrast to the temperature dependence of the same parameters for the parent $LaCoO_3$ compound. In our previous work [8], we showed that in this sample the sudden increase of Co-O bond length and MSD below 50 K was due to the mixture of HS and LS states. Therefore, for the $La_{0.75}Ba_{0.25}CoO_{2.9}$ sample at low temperatures the majority of Co ions are in a HS state with a minor inclusion of conducting IS states responsible for the formation of FM clusters evident from magnetization, resistivity, and neutron-diffraction measurements. We now take this HS-dominated AFM state of $La_{0.75}Ba_{0.25}CoO_{2.9}$ at 2 K and ambient pressure and discuss how the spin-states are changing with applied pressure and increased temperature.

At relatively low pressures ($V > 10.83$ Å^3/atom), all cobalt ions are always in the HS state with the magnitude of the magnetic moment per cobalt atom near 3.1 μ_B. Our calculations show that at $V = 10.83$ Å^3/atom, only half of Co ions have HS configuration, while the other half are in an IS state. When the system is further compressed below $V = 10.83$ Å^3/atom, HS states transform into IS states, leaving only one of eight of Co ions in a HS state. Finally, the first structural transition from $R\bar{3}c$ (AFM) to $Pm\bar{3}m$ (AFM) occurs near $V = 10.6$ Å^3/atom. With further increase of the pressure, the magnetic transition from AFM to FM in $Pm\bar{3}m$ is taking place at about $V = 10.3$ Å^3/atom. In the interval $V = 10.3 - 9.26$ Å^3/atom, all Co ions are in an IS state and system has a tendency toward orbital ordering, which stabilizes the FM phase [9]. Increasing pressure leads to the emerging of the LS states at some of the Co sites. The change of the spin-state of Co ions is not happening simultaneously; thus different ions exist in different states at the same pressure, i.e., a mixture of IS and LS states begins to form. As pressure continues to increase, the concentration of the LS states is increasing, ultimately leading to the NM state below $V = 9.25$ Å^3/atom (45 GPa). Our picture of magnetic and spin-state transitions agrees well with experimental studies of the cubic cobaltites with a barium concentration of 0.5, 0.55, and 0.6 [17,57,58], which showed that the FM ordering corresponds to an IS/LS mixture, while the AFM one corresponds to a HS/LS mixture.

It is worth noting that the transition to the NM state in $La_{0.75}Ba_{0.25}CoO_{2.9}$ is slowed down as compared with the parent compound $LaCoO_3$ due to nonstoichiometry and oxygen deficiency, both contributing to the chemical inhomogeneities in $La_{0.75}Ba_{0.25}CoO_{2.9}$ [17,57–59]. In particular, the oxygen deficiency contributes to the appearance of additional holes. The localization of these holes makes the magnetic moment-bearing states more energetically favorable and hence the transition to the NM state occurs at higher pressure as compared with $LaCoO_3$.

V. CONCLUSIONS

The possibility of engineering new materials by doping $LaCoO_3$ cobaltite is rather appealing, despite some structural and magnetic properties of the parent compound that are still under debate. Relating macroscopic magnetic properties to the spin-state transitions on atomic scale is not straightforward and requires a combined approach of experimental and calculational methods. Such approach was applied to study magnetic and structural phase transitions of $La_{0.75}Ba_{0.25}CoO_{2.9}$ compound under pressure. Application of pressure provides an additional parameter for manipulation of $La_{0.75}Ba_{0.25}CoO_{2.9}$ properties and opens novel opportunities for designing materials of the future.

Using neutron and x-ray scattering diffraction methods, we establish that at 50 K and at ambient pressure, $La_{0.75}Ba_{0.25}CoO_{2.9}$ is a mixture of 73% rhombohedral phase with the space group $R\bar{3}c$ and 27% cubic phase with the space group $Pm\bar{3}m$. The rhombohedral phase is AFM with all spins in a HS state. The cubic phase is a mixture of a dominant AFM phase with HS states and FM clusters, which appear from thermally induced IS states. Because the Co ionic radii in HS and IS states are different (0.61 and 0.54 Å), the cubic phase is easier to compress than the rhombohedral phase, which is fully populated with HS states with the same ionic radius. With application of pressure, the rhombohedral phase transforms into the cubic one. A relatively sharp rhombohedral to cubic phase transition is clearly visible from the experimental data at 50 K at about 10 GPa. This transition occurs at lower pressures with an increase of the temperature. The DFT+U calculations were used to study magnetic and structural transitions at 0 K as a function of applied pressure. In agreement with our experimental results, the structural transition from rhombohedral to cubic phase was found at about 10 GPa, while long-range AFM order has been retained. No further structural transitions from the cubic phase were evident with increase of the pressure; however, AFM to FM phase transition was observed at 16 GPa. This indicates the gradual change from nonconducting HS states into IS states, responsible for development of FM order in the pressure range between 16 and 45 GPa. Above 45 GP, the magnetic order is completely suppressed, indicative of all ions in a LS state. Our model of pressure-induced spin-state transitions in $La_{0.75}Ba_{0.25}CoO_{2.9}$ compound will benefit from additional neutron-scattering measurements at pressures above 16 GPa. These measurements will be pursued at existing [60] and future [61] spallation neutron sources.

[1] P. G. Radaelli and S. W. Cheong, Phys. Rev. B **66**, 094408 (2002).

[2] G. Maris, Y. Ren, V. Volotchaev, C. Zobel, T. Lorenz, and T. T. M. Palstra, Phys. Rev. B **67**, 224423 (2003).

[3] D. Louca and J. L. Sarrao, Phys. Rev. Lett. **91**, 155501 (2003).

[4] D. Phelan, D. Louca, S. Rosenkranz, S.-H. Lee, Y. Qiu, P. J. Chupas, R. Osborn, H. Zheng, J. F. Mitchell, J. R. D. Copley, J. L. Sarrao, and Y. Moritomo, Phys. Rev. Lett. **96**, 027201 (2006).

[5] D. P. Kozlenko, N. O. Golosova, Z. Jirak, L. S. Dubrovinsky, B. N. Savenko, M. G. Tucker, Y. Le Godec, and V. P. Glazkov, Phys. Rev. B **75**, 064422 (2007).

[6] N. Sundaram, Y. Jiang, I. E. Anderson, D. P. Belanger, C. H. Booth, F. Bridges, J. F. Mitchell, T. Proffen, and H. Zheng, Phys. Rev. Lett. **102**, 026401 (2009).

[7] Y. Jiang, F. Bridges, N. Sundaram, D. P. Belanger, I. E. Anderson, J. F. Mitchell, and H. Zheng, Phys. Rev. B **80**, 144423 (2009).

[8] M. Feygenson, D. Novoselov, S. Pascarelli, R. Chernikov, O. Zaharko, F. Porcher, D. Karpinsky, A. Nikitin, D. Prabhakaran, A. Sazonov, and V. Sikolenko, Phys. Rev. B **100**, 054306 (2019).

[9] M. A. Korotin, S. Y. Ezhov, I. V. Solovyev, V. I. Anisimov, D. I. Khomskii, and G. A. Sawatzky, Phys. Rev. B **54**, 5309 (1996).

[10] F. Fauth, E. Suard, and V. Caignaert, Phys. Rev. B **65**, 060401(R) (2001).

[11] V. Sikolenko, V. Efimov, I. O. Troyanchuk, D. V. Karpinsky, M. V. Bushinsky, and D. Sheptyakov, J. Phys.: Conf. Ser. **391**, 012106 (2012).

[12] A. P. Sazonov, I. O. Troyanchuk, H. Gamari-Seale, V. V. Sikolenko, K. L. Stefanopoulos, G. K. Nicolaides, and Y. K. Atanassova, J. Phys.: Condens. Matter **21**, 156004 (2009).

[13] I. O. Troyanchuk, D. V. Karpinsky, M. V. Bushinsky, V. Sikolenko, V. Efimov, and A. Cervellino, JETP Lett. **93**, 139 (2011).

[14] P. Tong, J. Yu, Q. Huang, K. Yamada, and D. Louca, Phys. Rev. Lett. **106**, 156407 (2011).

[15] I. Fita, R. Szymczak, R. Puzniak, I. O. Troyanchuk, J. Fink-Finowicki, Ya. M. Mukovskii, V. N. Varyukhin, and H. Szymczak, Phys. Rev. B **71**, 214404 (2005).

[16] I. Fita, R. Szymczak, R. Puzniak, A. Wisniewski, I. O. Troyanchuk, D. V. Karpinsky, V. Markovich, and H. Szymczak, Phys. Rev B **83**, 064414 (2011).

[17] I. O. Troyanchuk, M. V. Bushinsky, V. Sikolenko, V. Efimov, C. Ritter, T. Hansen, and D. M. Többens, Eur. Phys. J. B **86**, 435 (2013).

[18] G. E. Sterbinsky, R. Nanguneri, J. X. Ma, J. Shi, E. Karapetrova, J. C. Woicik, H. Park, J.-W. Kim, and P. J. Ryan, Phys. Rev. Lett. **120**, 197201 (2018).

[19] S. K. Pandey, Ashwani Kumar, S. Patil, V. R. R. Medicherla, R. S. Singh, K. Maiti, D. Prabhakaran, A. T. Boothroyd, and A. V. Pimpale, Phys. Rev B **77**, 045123 (2008).

[20] J. Kuneš, V. I. Anisimov, A. V. Lukoyanov, and D. Vollhardt, Phys. Rev B **76**, 165115 (2007).

[21] V. Křápek, P. Novák, J. Kuneš, D. Novoselov, D. M. Korotin, and V. I. Anisimov, Phys. Rev. B **86**, 195104 (2012).

[22] H. Park, R. Nanguneri, and A. T. Ngo, Phys. Rev. B **101**, 195125 (2020).

[23] M. Karolak, M. Izquierdo, S. L. Molodtsov, and A. I. Lichtenstein, Phys. Rev. Lett. **115**, 046401 (2015).

[24] B. Amadon, F. Lechermann, A. Georges, F. Jollet, T. O. Wehling, and A. I. Lichtenstein, Phys. Rev. B **77**, 205112 (2008).

[25] L. Craco and E. Müller-Hartmann, Phys. Rev. B **77**, 045130 (2008).

[26] R. Eder, Phys. Rev. B **81**, 035101 (2010).

[27] H. Hsu, K. Umemoto, M. Cococcioni, and R. Wentzcovitch, Phys. Rev. B **79**, 125124 (2009).

[28] B. Chakrabarti, T. Birol, and K. Haule, Phys. Rev. Materials **1**, 064403 (2017).

[29] P. Dutta, S. Lal, and S. K. Pandey, Eur. Phys. J. B **91**, 183 (2018).

[30] N. Benayad, M. Djermouni, A. Zaoui, S. Kacimi, and A. Boukortt, Mater. Chem. Phys. **207**, 507 (2018).

[31] J. Hejtmánek, Z. Jirák, K. Kníek, M. Maryško, M. Veverk, and H. Fujishiro, J. Magn. Magn. Mater. **272**, E283 (2004).

[32] J. Maria, S. Nazir, S. M. Alay-e-Abbas, and A. Shaukat, J. Magn. Magn. Mater. **368**, 230 (2014).

[33] A. S. Panfilov, G. E. Grechnev, A. A. Lyogenkaya, V. A. Pashchenko, I. P. Zhuravleva, L. O. Vasylechko, V. M. Hreb, V. A. Turchenko, and D. Novoselov, Phys. B: Condens. Matter **553**, 80 (2019).

[34] V. V. Sikolenko, S. L. Molodtsov, M. Izquierdo, I. O. Troyanchuk, D. Karpinsky, S. I. Tiutiunnikov, E. Efimova, D. Prabhakaran, D. Novoselov, and V. Efimov, Phys. B: Condens. Matter **536**, 597 (2018).

[35] D. M. Korotin, D. Novoselov, and V. I. Anisimov, J. Phys.: Condens. Matter **26**, 195602 (2014).

[36] D. Korotin, V. Kukolev, A. V. Kozhevnikov, D. Novoselov, and V. I. Anisimov, J. Phys.: Condens. Matter **24**, 415603 (2012).

[37] D. Novoselov, D. M. Korotin, and V. I.Anisimov, JETP Lett. **103**, 573 (2016).

[38] A. Jaffe, Y. Lin, and H. I. Karunadasa, ACS Energy Lett. **2**, 1549 (2017).

[39] S. Liu, S. Sun, C. K. Gan, A. Granados del Aguila, Y. Fang, J. Xing, T. T Ha Do, T. J. White, H. Li, W. Huang, and Q. Xiong, Sci. Adv. **5**, eaav9445 (2019).

[40] L. Kong, G. Liu, J. Gong, L. Mao, M. Chen, Q. Hu, X. Lü, W. Yang, M. G. Kanatzidis, and H. Mao, Proc. Natl. Acad. Sci. USA **117**, 16121 (2020).

[41] I. O. Troyanchuk, M. V. Bushinsky, A. V. Nikitin, L. S. Lobanovsky, A. M. Balagurov, V. Sikolenko, and V. Efimov, and D. V. Sheptyakov, J. Appl. Phys. **113**, 053909 (2013).

[42] V. Sikolenko, V. Efimov, D. Többens, S. Schorr, C. Ritter, M. Bushinsky, and I. O. Troyanchuk, Powder Diffr. **28**, S126 (2013).

[43] G. Vankó, J. P. Rueff, A. Mattila, Z. Németh, and A. Shukla, Phys. Rev. B **73**, 024424 (2006).

[44] V. Sikolenko, I. O. Troyanchuk, M. V. Bushinsky, D. V. Karpinsky, V. Efimov, C. Ritter, S. Schorr, M. V. Silibin, A. A. Dronov, K. N. Nekludov, S. A. Gavrilov, and F. R. Schilling, Mater. Chem. Phys. **181**, 78 (2016).

[45] V. V. Sikolenko, A. P. Sazonov, I. O. Troyanchuk, D. Többens, U. Zimmermann, E. V. Pomjakushina, and H. Szymczak, J. Phys.: Condens. Matter **16**, 7313 (2004).

[46] G. Kresse and J. Furthmüller, Phys. Rev. B **54**, 11169 (1996).

[47] A.-H. Lu, E. L. Salabras, and F. Schuth, Angew. Chem. Int. Ed. **46**, 1222 (2007).

[48] V. Skumryev, S. Stoyanov, Y. Zhang, G. Hadjipanayis, D. Givord, and J. Nogues, Nature (London) **423**, 850 (2003).

[49] R. Lengsdorf, M. Ait-Tahar, S. S. Saxena, M. Ellerby, D. I. Khomskii, H. Micklitz, T. Lorenz, and M. M. Abd-Elmeguid, Phys. Rev. B **69**, 140403(R) (2004).

[50] E. O. Wollan and W. C. Koehler, Phys. Rev. **100**, 545 (1955).

[51] A. K. Kundu, E. L. Rautama, P. Boullay, V. Caignaert, V. Pralong, and B. Raveau, Phys. Rev. B **76**, 184432 (2007).

[52] P. Mandal, P. Choudhury, S. K. Biswas, and B. Ghosh, Phys. Rev. B **70**, 104407 (2004).

[53] D. Garcés, C. F. Setevich, A. Caneiro, G. Julio Cuello, and L. Mogni, J. Appl. Cryst. **47**, 325 (2014).

[54] J. Wu, J. W. Lynn, C. J. Glinka, J. Burley, H. Zheng, J. F. Mitchell, and C. Leighton, Phys. Rev. Lett. **94**, 037201 (2005).

[55] W. Luo and F. Wang, J. Magn. Magn. Mater. **321**, 1280 (2009).

[56] J. Wu and C. Leighton, Phys. Rev. B **67**, 174408 (2003).

[57] I. O. Troyanchuk, M. V. Bushinsky, V. V. Sikolenko, and C. Ritter, J. Exp. Theor. Phys. **128**, 98 (2019).

[58] I. Troyanchuk, M. Bushinsky, N. Tereshko, C. Ritter, V. Sikolenko, and M. Silibin, Phys. Status Solidi B **255**, 1800315 (2018).

[59] J. Buckeridge, F. H. Taylor, and C. R. A. Catlow, Phys. Rev. B **93**, 155123 (2016).

[60] O. Arnold, J. C. Bilheux, J. M. Borreguero, A. Buts, S. I. Campbell, L. Chapon, M. Doucet, N. Draper, R. Ferraz Leal, M. A. Gigg, V. E. Lynch, A. Markvardsen, D. J. Mikkelson, R. L. Mikkelson, R. Miller, K. Palmen, P. Parker, G. Passo, T. G. Perring, P. F. Peterson, S. Ren *et al.*, Nucl. Instrum. Methods Phys. Res. Sect. A **764**, 156 (2014).

[61] K. H. Andersen, D. N. Argyriou, A. J. Jackson, J. Houston, P. F. Henry, P. P. Deen, R. Toft-Petersen, P. Beran, M. Strobl, T. Arnold *et al.*, Nucl. Instrum. Methods Phys. Res. Sec. A **957**, 163402 (2020).